



ELSEVIER

Available online at www.sciencedirect.com

SCIENCE @ DIRECT®

International Journal of Solids and Structures 42 (2005) 6643–6661

INTERNATIONAL JOURNAL OF
**SOLIDS and
STRUCTURES**

www.elsevier.com/locate/ijsolstr

Strength optimization of metallic sandwich panels subject to bending

H.J. Rathbun, F.W. Zok *, A.G. Evans

Materials Department, University of California, Santa Barbara, CA 93106-5050, United States

Received 3 August 2004; received in revised form 16 June 2005
Available online 15 August 2005

Abstract

A general methodology for the design of strong, lightweight sandwich panels is described and implemented. Several core topologies are considered, including square-section truss members in pyramidal and tetrahedral configurations, square honeycombs, and corrugated sheets. When the number of independent design parameters is restricted to three, closed-form analytical solutions for the optimal design are obtained. Alternatively, when a fourth parameter is added (as needed to fully characterize the panel geometry), numerical routes are required. The results demonstrate that the three parameter optimizations yield design weights that are only slightly heavier than those of the fully optimized panels, provided the value of the fourth parameter is selected judiciously. The weight rankings of the various core topologies change with load capacity, although the differences between them are generally small, particularly upon comparison with the weight of a solid panel.

© 2005 Elsevier Ltd. All rights reserved.

Keywords: Sandwich panels; Lightweight structures; Optimal design

1. Introduction

Metallic sandwich structures have recently been investigated for their lightweight and multifunctional characteristics, as well as their resistance to blast (Evans et al., 2001; Hutchinson et al., 2003; Qiu et al., 2003; Xue and Hutchinson, 2003; Fleck and Deshpande, 2004). Various cores have been described, including tetrahedral and pyramidal truss configurations, square honeycombs, corrugated and diamond prismatic configurations and textiles. Methods for manufacturing panels with these cores have been invented and described (Sypeck and Wadley, 2002; Wadley et al., 2003). In some cases, tests have been performed to

* Corresponding author. Tel.: +1 805 893 8699; fax: +1 805 893 8486.
E-mail address: zok@engineering.ucsb.edu (F.W. Zok).

characterize the core properties and, in others, sandwich panels with these cores have been tested in various shear and bending modes (Deshpande and Fleck, 2001; Chiras et al., 2002; Rathbun et al., 2004; Cote et al., 2004). In most cases, analytical formulae characterizing the elastic properties of the cores and of the loads at which they yield and buckle have been derived (Lu et al., 2001; Wicks and Hutchinson, 2001, 2004; Deshpande et al., 2001). These formulae have been used to plot failure mechanism maps and to identify minimum weight designs of the corresponding panels. A relatively complete characterization of the performance of both the cores and the panels, involving both calculations and measurements, has been presented in only one case: pyramidal truss cores (Zok et al., 2004). Even then, the results have been restricted to yield strain, ε_y , and strain hardening levels representative of annealed stainless steel. None of the articles have attempted an explicit comparison among all available core topologies for materials with a range of ε_y . This article addresses one basic aspect of this comparison, by establishing minimum weight designs for each, subject to generalized bending.

Application of the design methodology is first demonstrated for one specific topology: the pyramidal truss core. This illustration reveals some of the trends in the active failure modes and their transitions with increasing applied load. It also serves to motivate the addition of a thickness restriction on the core, to ensure that the designs remain in the domain of thin plates. The optimization methodology is then generalized to other core topologies, including tetrahedral truss, square honeycomb, and corrugated sheet. Comparisons of weights are used to assess the merits of the various core topologies.

2. Geometry and loading

Optimizations are performed for sandwich panels subject to generalized bending (Fig. 1), with maximum moment M and maximum transverse shear V (both per unit width). The pertinent load index Π for strength-based designs is (Ashby et al., 2000)¹

$$\Pi = \frac{V^2}{EM} \quad (1)$$

where E is Young's modulus. The ratio of the maximum M and V defines a characteristic length scale, $\ell \equiv M/V$ (Wicks and Hutchinson, 2001). The non-dimensional weight index is (Ashby et al., 2000)

$$\Psi = \frac{W}{\rho\ell} \quad (2)$$

where W is the structural weight per unit area and ρ the density of the solid material. Designs that minimize weight, Ψ , for specified load, Π , are found by establishing the load capacity for all possible failure modes, within the core as well as the faces, and then varying the dimensions to determine the lowest weight (Ashby et al., 2000).

The cores illustrated in Fig. 2 represent prototypical topologies of current interest. Two of these are examples of truss-based cores, in tetrahedral and pyramidal configurations (Fig. 2(a) and (b)). The other two are based on plate elements in prismatic configurations; specifically, square honeycomb and corrugated sheet (Fig. 2(c) and (d)).² All panel configurations can be manufactured using established cutting, bending and bonding procedures (Sypeck and Wadley, 2002; Wadley et al., 2003; Rathbun et al., 2004; Zok et al., 2004). In general, each panel geometry is characterized by four independent parameters: face sheet

¹ This index is the square of that defined in previous articles on sandwich panels (Wicks and Hutchinson, 2001; Zok et al., 2003). The present one is preferred since it is directly proportional to load, rather than to the square root of load.

² Analyses of hexagonal honeycomb core panels have been performed also, and the results found to be almost indistinguishable from those of the square honeycomb cores. Consequently, the results for the hexagonal honeycombs are not presented here.

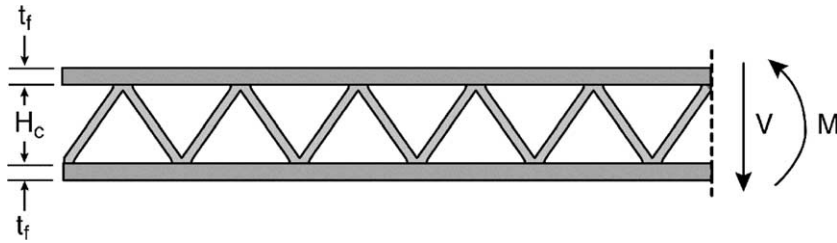


Fig. 1. Schematic showing generalized bending loads acting on a sandwich panel.

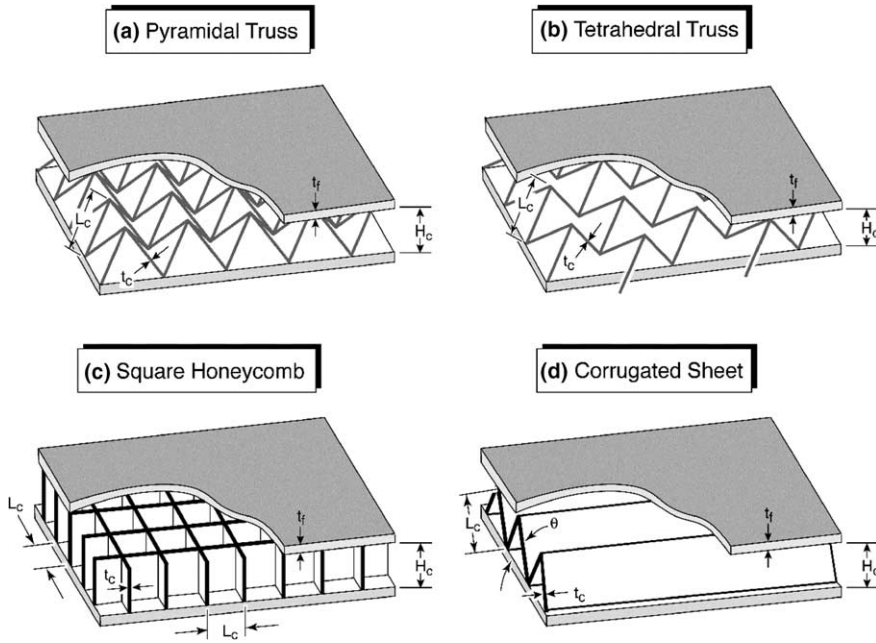


Fig. 2. Schematics of sandwich panels with the four prototypical core topologies. Bending loads are applied along the long (horizontal) axis.

thickness, t_f , core thickness, H_c , core member thickness, t_c , and core member length, L_c . When normalized by the characteristic length scale, ℓ , the first three of these form non-dimensional parameters defined by

$$\lambda_c \equiv t_c/\ell \tag{3}$$

$$\lambda_f \equiv t_f/\ell \tag{4}$$

$$A_c \equiv H_c/\ell \tag{5}$$

The fourth non-dimensional parameter is defined as the ratio ξ of core member length to core thickness

$$\xi \equiv L_c/H_c \tag{6}$$

For all but the honeycomb core, a fifth (dependent) parameter can also be identified: the angle θ between the core members and the face sheets, given by

$$\theta = \sin^{-1}(H_c/L_c) = \sin^{-1}(1/\xi) \tag{7}$$

To keep the analysis tractable, the cores are chosen to have specific orientations with respect to the bending loads, as illustrated in Fig. 2. For the corrugated sheet core, loadings both parallel and perpendicular to the direction of corrugation are considered.

3. Optimization of pyramidal truss core panel

As a prelude to the generalized methodology, the optimization procedure is illustrated for the specific case of a pyramidal truss core panel. It begins with a stress analysis of both the core members and the face sheets coupled with failure criteria based on yielding (at a critical value of tension or compression) and buckling (in accordance with the Euler formula). To ensure conservative designs, the rotational constraints both of the face sheets on the core members and of the core members on the face sheets are neglected. That is, all connections are treated as pinned joints. Comparisons with numerical simulations in which the connections are assumed to be rigid reveal only slight differences in panel strength (Zok et al., 2004, in press). It is further assumed that the core members carry all of the transverse shear and the face sheets carry all of the bending moment. An assessment of the latter assumptions is made elsewhere (Rathbun et al., in preparation).

The four possible failure modes are face yielding (FY), face buckling (FB), core yielding (CY) and core buckling (CB) (Ashby et al., 2000). Each leads to a constraint in the optimization. For the pyramidal truss core panel, the constraints are

$$\Pi \frac{A_c^{-1} \lambda_f^{-1}}{\varepsilon_y} \leq 1 \quad (\text{face yielding}) \quad (8a)$$

$$\Pi \frac{24(1 - \nu^2) A_c \lambda_f^{-3}}{\pi^2 \tan^2 \theta} \leq 1 \quad (\text{face buckling}) \quad (8b)$$

$$\Pi \frac{\sqrt{2} A_c \lambda_c^{-2}}{2 \varepsilon_y \sin \theta \tan \theta} \leq 1 \quad (\text{core yielding}) \quad (8c)$$

$$\Pi \frac{6\sqrt{2} A_c^3 \lambda_c^{-4}}{\pi^2 \sin^3 \theta \tan \theta} \leq 1 \quad (\text{core buckling}) \quad (8d)$$

A failure mode is considered active when the associated constraint function reaches unity. From geometry, the corresponding non-dimensional weight is

$$\Psi = 2\lambda_f + \frac{2\lambda_c^2 \tan^2 \theta}{A_c \sin \theta} \quad (9)$$

It is noteworthy that, in general, the constraint functions and the weight index exhibit power law scalings with the independent geometric parameters: a feature exploited later in the generalized optimization methodology.

The objective of the optimization is to find the geometric parameters that minimize weight, Ψ , for a prescribed load, Π . In general, the optima are obtained at the confluence of three failure mechanisms (Wicks and Hutchinson, 2001; Zok et al., 2003, 2004). With a total of four such mechanisms, four candidate combinations of active mechanisms exist, summarized in Table 1. If one of the parameters is fixed, the number of independent geometric parameters is reduced to *three*. Consequently, once the three pertinent constraint functions are set equal to unity, the values of all parameters are uniquely defined. As demonstrated below, the latter results can be expressed through explicit analytical formulae. Otherwise, to retain generality (with *four* independent parameters), the optima are obtained by eliminating three parameters via the pertinent constraint functions, expressing the weight in terms of the remaining independent parameter,

Table 1
Candidate combinations of constraint functions

Candidate #	Constraints active
I	FY–FB–CB
II	FB–CB–CY
III	FY–CB–CY
IV	FY–FB–CY

x , and then setting $\partial\Psi/\partial x = 0$. As illustrated in Appendix A, the latter optimizations often lead to implicit functions for the geometric parameters and the weight. Although solutions for these functions can be obtained through standard numerical routes, the trends in the optimal configuration with the parameters of interest (e.g., load and yield strain) are not as transparent as they are in the explicit analytical formulae stemming from the three-parameter optimizations. As a consequence, only the latter analytical formulae are presented here. An assessment of these formulae is made through select comparisons with numerical results from the four-parameter optimizations, presented in Section 6.

The three-parameter optimization proceeds in four steps. (i) One parameter, ξ , is fixed. This precludes determination of its optimal value at each load level. However, in subsequent calculations, its magnitude can be varied systematically to assess its effect on weight over the pertinent load range. Alternatively, the selection of ξ can be guided by numerical solutions from the full (four-parameter) optimization, presented later. (ii) Solutions for the remaining independent parameters, λ_c , λ_f and λ_e , are obtained for each of the four candidate combinations of active mechanisms shown in Table 1. This is accomplished by setting the three associated constraint functions in Eq. 8 equal to unity. (iii) The admissibility of a candidate solution is determined by evaluating the remaining fourth constraint function. If the latter value falls below unity, the solution is considered admissible; that is, it does not violate the assumption that the three assumed mechanisms are indeed the only active ones. Conversely, if the fourth constraint function exceeds unity, the solution is inadmissible. (iv) Among the admissible solutions, the one that yields the lowest weight defines the optimal design.

Implementation of the second step of this methodology for the pyramidal truss core panel yields the results shown in Table 2. Here, solutions for the three geometric parameters and the panel weight for each of the four candidate mechanism combinations are summarized. Representative results are plotted in Fig. 3: solid and dashed curves denoting admissible and inadmissible solutions, respectively. At low loads, two

Table 2
Solutions pertinent to three-parameter optimization of pyramidal truss core sandwich panel

Candidate #	Core thickness, λ_c	Face sheet thickness, λ_f	Core member thickness, λ_e	Weight, Ψ
I	$\left(\frac{\pi^2}{24(1-v^2)\epsilon_y^3}\right)^{1/4} \Pi^{1/2}$	$\left(\frac{24(1-v^2)}{\pi^2\epsilon_y}\right)^{1/4} \Pi^{1/2}$	$\left(\frac{24}{\pi^2(1-v^2)^3\epsilon_y^9}\right)^{1/16} \Pi^{5/8}$	$\left(\frac{384(1-v^2)}{\pi^2\epsilon_y}\right)^{1/4} \Pi^{1/2}$ $+9.3\left[\frac{1}{(1-v^2)\pi^6\epsilon_y^3}\right]^{1/8} \Pi^{3/4}$
II	$\frac{\pi^2}{24\epsilon_y^2} \Pi$	$\left[\frac{(1-v^2)^2}{\epsilon_y^4}\right]^{1/6} \Pi^{2/3}$	$\frac{\pi}{\sqrt{24\epsilon_y^3}} \Pi$	$\left[\frac{64(1-v^2)^2}{\epsilon_y^4}\right]^{1/6} \Pi^{2/3} + \frac{2\sqrt{2}}{\epsilon_y} \Pi$
III	$\frac{\pi^2}{24\epsilon_y^2} \Pi$	$\frac{24\epsilon_y}{\pi^2}$	$\frac{\pi}{\sqrt{24\epsilon_y^3}} \Pi$	$\frac{48\epsilon_y}{\pi^2} + \frac{2\sqrt{2}}{\epsilon_y} \Pi$
IV	$\left(\frac{\pi^2}{24(1-v^2)\epsilon_y^3}\right)^{1/4} \Pi^{1/2}$	$\left(\frac{24(1-v^2)}{\pi^2\epsilon_y}\right)^{1/4} \Pi^{1/2}$	$\left(\frac{\pi^2}{24(1-v^2)\epsilon_y^7}\right)^{1/8} \Pi^{3/4}$	$\left(\frac{384(1-v^2)}{\pi^2\epsilon_y}\right)^{1/4} \Pi^{1/2} + \frac{2\sqrt{2}}{\epsilon_y} \Pi$

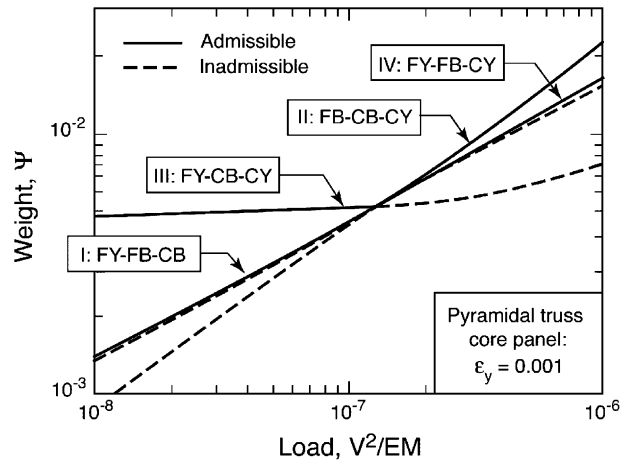


Fig. 3. Illustration of the methodology used to ascertain the optimal design. Each curve represents a candidate solution to the optimization, based on the confluence of three failure mechanisms. Solid and dashed curves represent admissible and inadmissible parts of the solutions, respectively. Among the two admissible solutions in each of the two loading domains (on either side of $V^2/EM \approx 10^{-7}$), the one that yields the higher load (or, equivalently, the lower weight) is optimal.

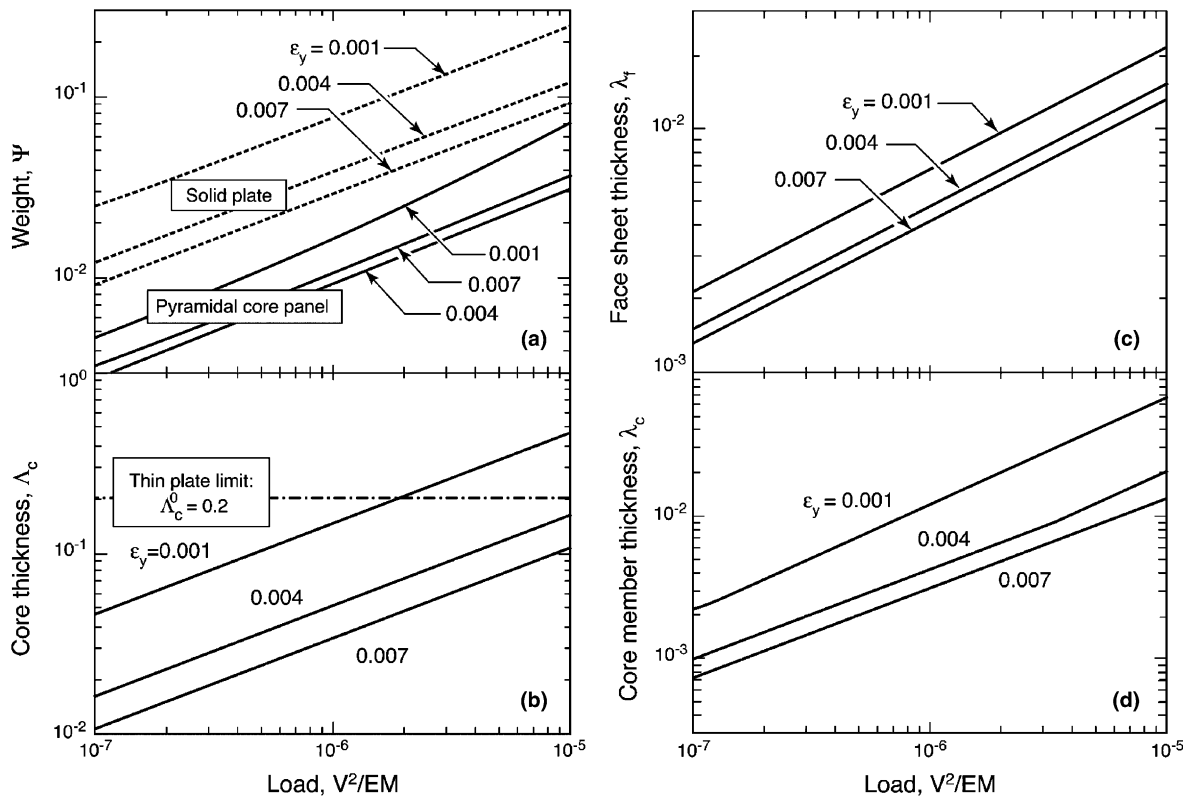


Fig. 4. Effects of yield strain on the optimal design of a pyramidal core sandwich panel ($\nu = 1/3$). Note that, for low yield strain materials, the core thickness increases rapidly with load, eventually departing the domain of thin plates.

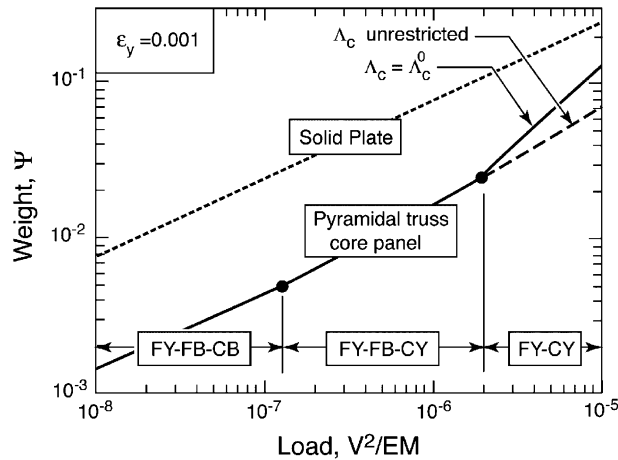


Fig. 5. Illustration of an optimization for a pyramidal truss core sandwich panel in which the core thickness is restricted to $A_c \leq A_c^0 = 0.2$. Transitions in active failure mechanisms are indicated by the solid symbols.

admissible solutions are obtained. Among them, the one that yields the lower weight involves FY, FB and CB (candidate I). Similarly, at high loads, two other admissible solutions are obtained, with the lower weight occurring for the combination of FY, FB and CY. Where the four solutions intersect, the active core mechanism changes from buckling to yielding; both face yielding and buckling are operative over the entire load range.

The effects of yield strain on the optimal designs are shown in Fig. 4. Also shown for comparison is the corresponding weight of a solid monolithic panel, given by (Zok et al., 2003)

$$\Psi = \left(\frac{6II}{\epsilon_y}\right)^{1/2} \tag{10}$$

The significant weight reduction for a pyramidal truss core sandwich panel over the equivalent weight monolithic panel as well as the beneficial effects of increasing yield strain are evident.

The results in Fig. 4(b) reveal that the core thickness, characterized by A_c , increases monotonically with load, eventually falling outside the domain of thin plates. To ensure suitably thin designs, an additional constraint is placed on the optimization: notably, $A_c \leq A_c^0$, where A_c^0 is the maximum allowable core thickness, taken to be 0.2. The effect of this restriction on the optimal design is illustrated in Fig. 5. In this case, the core-thickness limit is attained in the domain in which FY, FB and CY are active. Thereafter, as the load increases but the core thickness remains fixed, FB is inactive; instead, failure occurs by a combination of only FY and CY. This produces three load domains, characterized by the active failure mechanisms indicated in Fig. 5. The critical loads associated with these transitions as well as the optimal values of the geometric parameters and the weight are given in a subsequent section.

4. Generalization of three-parameter optimization

The same methodology has been used to optimize the other panel configurations shown in Fig. 2. Solutions for the constraint functions have either been taken from previous articles (Zok et al., 2003; Wicks and Hutchinson, 2001; Lu et al., 2001) or derived using similar methods. Inspection reveals that all solutions can be reduced to the following common forms.

Since FY is independent of the core, the associated constraint function is identical to that given in Eq. (8a). For the other mechanisms, the constraint functions must be altered to account for the effects of core topology. In general, they can be expressed as

$$\Pi h(\xi, \nu) A_c \lambda_f^{-3} \leq 1 \quad (\text{face buckling}) \quad (11)$$

$$\frac{\Pi f(\xi) A_c^c \lambda_c^{-b}}{\varepsilon_y} \leq 1 \quad (\text{core yielding}) \quad (12)$$

$$\Pi g(\xi, \nu) A_c^l \lambda_c^{-k} \leq 1 \quad (\text{core buckling}) \quad (13)$$

The non-dimensional functions $h(\xi, \nu)$, $f(\xi)$ and $g(\xi, \nu)$ and the exponents b , c , k and l are governed by core topology. Their magnitudes are summarized in Table 3. The corresponding non-dimensional weight is

$$\Psi = 2\lambda_f + m(\xi) \lambda_c^n A_c^{1-n} \quad (14)$$

Pertinent values of $m(\xi)$ and n are also given in Table 3. Henceforth, the three-parameter optimization proceeds in the manner described above for the pyramidal truss core panel. That is, solutions for the four candidate mechanism combinations are obtained, their admissibility is assessed, and the admissible solution that yields the lowest weight is used to obtain the optimal design. Furthermore, at high loads, the core thickness is restricted to $A_c \leq A_c^0$.

By analogy to the trends obtained for the pyramidal core sandwich panels (Fig. 3), the loading range for all core topologies can be divided into three domains, hereafter referred to as low, intermediate, and high. The nature of the transitions between domains is illustrated in Fig. 6 and described below.

Table 3
Non-dimensional functions and exponents for constraint functions

		Topologies				
		Truss		Prismatic		
		Pyramidal	Tetrahedral	Square honeycomb	Corrugated transverse	Corrugated longitudinal
Core yield	b	2	2	1	1	1
	c	1	1	0	0	0
	$f(\xi)$	$\frac{\sqrt{2}}{2 \sin \theta \tan \theta}$	$\frac{\sqrt{3}}{\sin \theta \tan \theta}$	$3\sqrt{3}\xi/2$	$\frac{1}{\sin \theta}$	$\frac{3\sqrt{3}}{2 \tan \theta}$
Core buckling	k	4	4	3	3	3
	l	3	3	2	2	2
	$g(\xi, \nu)$	$\frac{6\sqrt{2}}{\Pi^2 \sin^3 \theta \tan \theta}$	$\frac{12\sqrt{3}}{\Pi^2 \sin^3 \theta \tan \theta}$	$\xi \leq 1: \frac{18(1-\nu^2)\xi^3}{\Pi^2(5.4+4\xi^2)}$ $\xi > 1: \frac{18(1-\nu^2)\xi^3}{\Pi^2(5.4\xi^2+4)}$	$\frac{12(1-\nu^2)}{\pi^2 \sin^3 \theta}$	$\frac{3(1-\nu^2)}{10 \sin^2 \theta \tan \theta}$
Face buckling	$h(\xi, \nu)$	$\frac{24(1-\nu^2)}{\Pi^2 \tan^2 \theta}$	$\frac{432(1-\nu^2)}{49 \Pi^2 \tan^2 \theta}$	$(1-\nu^2)\xi^2/3.3$	$\frac{48(1-\nu^2)}{\Pi^2 \tan^2 \theta}$	$\frac{4(1-\nu^2)}{3.3 \tan^2 \theta}$
Weight function	n	2	2	1	1	1
	$m(\xi)$	$\frac{2 \tan^2 \theta}{\sin \theta}$	$\frac{2\sqrt{3} \tan^2 \theta}{3 \sin \theta}$	$2/\xi$	$\frac{1}{\cos \theta}$	$\frac{1}{\cos \theta}$

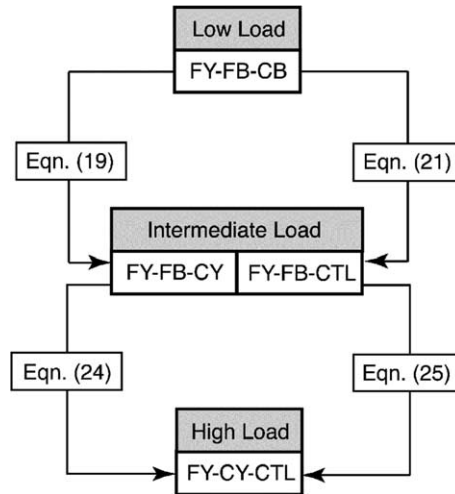


Fig. 6. Transitions in active constraints in three-parameter optimization (FY—face yielding; FB—face buckling; CB—core buckling; CY—core yielding; CTL—core thickness limit).

In the low load domain, the active failure mechanisms are always FY, FB and CB. The transition to intermediate loads occurs in one of two ways: (i) by a change in core failure mechanism, from CB to CY (as found for the pyramidal truss core), or (ii) by attainment of the core thickness limit (CTL), $A_c = A_c^0$. In the latter case, restriction of the core thickness to the critical value renders FB inactive, leaving only FY and CB. For these two scenarios, the transition to the high load domain occurs, respectively, when: (i) the core thickness limit is attained, whereupon CB becomes inactive and failure occurs by FY and CY, or (ii) the core failure mechanism changes from CB to CY, resulting, again, in a combination of FY and CY. The pertinent solutions for the optimal designs and the critical loads at which the transitions occur are summarized below.

4.1. Low load domain

As previously noted, the active failure mechanisms at low loads are always FY, FB and CB. Setting the constraints in Eqs. (8a), (11) and (13) equal to unity yields the optimal geometric parameters, given by

$$A_c = \left[\frac{\Pi^2}{\epsilon_y^3 h(\zeta, \nu)} \right]^{1/4} \tag{15a}$$

$$\lambda_f = \left[\frac{h(\zeta, \nu) \Pi^2}{\epsilon_y} \right]^{1/4} \tag{15b}$$

$$\lambda_c = \left[\frac{\Pi^{2(l+2)} g(\zeta, \nu)^4}{h(\zeta, \nu)^l \epsilon_y^{3l}} \right]^{1/4k} \tag{15c}$$

The corresponding weight, from Eq. (9), is

$$\Psi = 2 \left[\frac{h(\zeta, \nu) \Pi^2}{\epsilon_y} \right]^{1/4} + m(\zeta) \left\{ \frac{g(\zeta, \nu)^{4n} \Pi^{2k(1-n)+2n(l+2)}}{[h(\zeta, \nu) \epsilon_y^3]^2} \right\}^{1/4k} \tag{16}$$

4.2. Intermediate load domain

The optimal design and associated weight at intermediate loads depend on the nature of the transition from the low load domain. When it occurs in accordance with scenario (i) above (i.e., by transition from CB to CY, with core thickness $A_c < A_c^0$), the optimal design is obtained by setting the constraints in Eqs. (8a), (12) and (13) equal to unity, yielding

$$A_c = \left[\frac{\Pi^2}{\varepsilon_y^3 h(\xi, \nu)} \right]^{1/4} \tag{17a}$$

$$\lambda_f = \left[\frac{h(\xi, \nu) \Pi^2}{\varepsilon_y} \right]^{1/4} \tag{17b}$$

$$\lambda_c = \left[\frac{\Pi^{2(2+c)} f(\xi)^4}{\varepsilon_y^{4+3c} h(\xi, \nu)^c} \right]^{1/4b} \tag{17c}$$

The corresponding weight is given by

$$\Psi = 2 \left[\frac{h(\xi, \nu) \Pi^2}{\varepsilon_y} \right]^{1/4} + m(\xi) \left\{ \frac{f(\xi)^{4n} \Pi^{2b(1-n)+2n(2+c)}}{\varepsilon_y^{n(4+3c)+3b(1-n)}} \right\}^{1/4b} \tag{18}$$

Upon setting the solutions in the two domains equal to one another, the critical load at the transition is obtained

$$\Pi^{tr} = \frac{g(\xi, \nu)^b}{f(\xi)^k \varepsilon_y^{k+3/2} h(\xi, \nu)^{1/2}} \tag{19}$$

Conversely, when the transition occurs by scenario (ii) (i.e., attainment of the critical core thickness, $A_c = A_c^0$, whereupon FB becomes inactive), the optimal values of the remaining independent parameters are found by setting $A_c = A_c^0$ and setting the constraint functions in Eqs. (8a) and (13) equal to unity. The resulting geometric parameters and weight are

$$\lambda_f = \frac{\Pi}{\varepsilon_y A_c^0} \tag{20a}$$

$$\lambda_c = \left[\Pi (A_c^0)^l g(\xi, \nu) \right]^{1/k} \tag{20b}$$

$$\Psi = \frac{2\Pi}{\varepsilon_y A_c^0} + m(\xi) \left[\Pi (A_c^0)^{k/n-1} g(\xi, \nu) \right]^{n/k} \tag{20c}$$

Setting the solutions in the two domains equal yields the critical load at the transition

$$\Pi^{tr} = \left[h(\xi, \nu) \varepsilon_y^3 \right]^{1/2} (A_c^0)^2 \tag{21}$$

The conditions under which the two transition types are obtained can be ascertained through comparisons of the pertinent values of core thickness: specifically, A_c at the CB to CY transition and the maximum allowable value, A_c^0 . Such a comparison yields a critical core thickness, A_c^{cr} , given by

$$A_c^{cr} = \frac{g(\xi, \nu)^{b/2} \varepsilon_y^{(3b-k)/4}}{h(\xi, \nu)^{1/2} f(\xi)^{k/2}} \tag{22}$$

When $A_c^{cr} > A_c^0$, CB to CY defines the transition. Otherwise ($A_c^{cr} < A_c^0$), the transition is dictated by the core thickness limit.

4.3. High load domain

In the high load domain, the active failure mechanisms are FY and CY (independent of the sequence of preceding transitions). Setting $A_c = A_c^0$ and the functions in Eqs. (8a) and (12) equal to unity yields the optimal geometric parameters and the weight

$$\lambda_f = \frac{\Pi}{\varepsilon_y A_c^0} \quad (23a)$$

$$\lambda_c = \left[\frac{\Pi (A_c^0)^c f(\xi)}{\varepsilon_y} \right]^{1/b} \quad (23b)$$

$$\Psi = \frac{\Pi}{\varepsilon_y} \left[\frac{2}{A_c^0} + m(\xi) f(\xi) \right] \quad (23c)$$

The transition from intermediate to high loads depends on the operative mechanisms in the intermediate load domain. When $A_c < A_c^0$ in the intermediate domain (failure occurring by a combination of FY, FB and CY), the transition to high loads occurs when

$$\Pi^{tr} = \left[h(\xi, \nu) \varepsilon_y^3 \right]^{1/2} (A_c^0)^2 \quad (24)$$

Otherwise, when the intermediate load domain is dictated by the core thickness restriction ($A_c = A_c^0$), the transition to high loads occurs at

$$\Pi^{tr} = A_c^0 g(\xi, \nu)^{b/2} \left[\frac{\varepsilon_y}{f(\xi)} \right]^{k/2} \quad (25)$$

5. Results from three-parameter optimizations

An assessment of performance of the optimized panels is made through comparisons of their weights. Representative results for $\varepsilon_y = 0.001$ are presented in Fig. 7(a). For reasons described later, ξ is taken to be 0.5 for the honeycomb core; for the other topologies, θ is taken to be 45° , such that $\xi = \sqrt{2}$ (via Eq. (7)). For each case, results are plotted only upto the point at which the core relative density reaches 10%; for greater values, the assumptions underpinning the stress analyses are not expected to be valid. For comparison, the weight of a solid plate is also plotted on this figure. Three features are noteworthy. (i) The weights of all sandwich panels are significantly lower than that of the solid plate: typically by about an order of magnitude. (ii) The ranking of the panels changes with increasing load. For instance, at low loads ($\Pi < 10^{-6}$), the weight rank, in decreasing order, is: transverse corrugated, pyramidal, longitudinal corrugated, tetrahedral, and square honeycomb. In contrast, at high loads, the transverse corrugated panel is the lightest whereas the one with the square honeycomb core is the heaviest. The implication is that the topologies that are inherently most resistant to buckling (pertinent at low loads) are also inherently least resistant to yielding (pertinent at high loads), and vice-versa. (iii) The differences in weights of the optimized panels decrease with increasing load. In the high load domain, the maximum difference is only about 20%.

Insights into the similarities of the weights of the optimized panels can be gleaned from examination of the solutions for two limiting cases. (i) In the high load domain, the contribution to weight from the face sheets (the first term on the right side of Eq. (23c)) dominates over the core contribution (the second term),

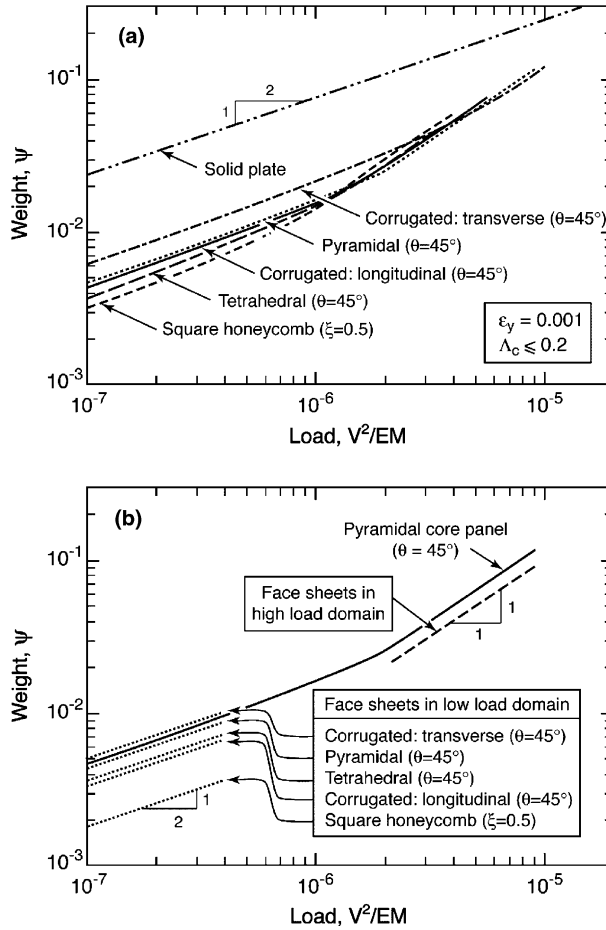


Fig. 7. (a) Results of three-parameter panel optimizations ($\nu = 1/3$). (b) Face sheet contributions to panel weight, in high and low load domains. For comparison, the weight of the pyramidal core panel is also shown.

typically by a factor of about 4. Moreover, the face contribution is *independent* of core topology and is given by

$$\Psi = \frac{2\Pi}{\varepsilon_y \Lambda_c^0} \tag{26}$$

This result is plotted in Fig. 7(b) and compared with the weight of the pyramidal core panel. (For clarity, results for other core topologies have been omitted.) The two correspond closely to one another: the differences representing the core contribution. Although the latter contributions vary by as much as a factor of 2 amongst the various core topologies, their magnitudes are always small in relation to that of the face sheets. Consequently, the optimal weight exhibits only a weak sensitivity to core topology. (ii) In the low load domain, the weight of the face sheets (given by the first term on the right side of Eq. (16)), is

$$\Psi = 2 \left[\frac{h(\zeta, \nu) \Pi^2}{\varepsilon_y} \right]^{1/4} \tag{27}$$

This term depends on core topology, through the function $h(\xi, \nu)$ (Table 2). Using the pertinent values of $h(\xi, \nu)$, the results of Eq. (27) are also plotted in Fig. 7(b). Here, again, the face sheet weight usually dominates, as evident from a comparison for the pyramidal core panel. Thus, differences in panel weights are attributable mainly to variations in face sheet contributions. The one exception is the square honeycomb panel, wherein the core contributes almost equal weight to that from the face sheets.

6. Four-parameter optimizations

To assess the preceding analytical solutions, full four-parameter optimizations have been performed. The constraints are those associated with failure, given by Eqs. (8a), (11), (12) and (13), as well as the core thickness restriction ($A_c \leq A_c^0$). Solutions for minimum weight (Eq. (14)) have been obtained numerically, using procedures described by Wicks and Hutchinson (2001). The optimal values of ξ for the honeycomb core panels and θ for the other panels are plotted in Fig. 8. Select analytical solutions for these parameters as well as the panel weights are summarized in Appendix A. The weights of the fully optimized panels are plotted in Fig. 9, along with the results from the three-parameter optimizations. Finally, Fig. 10 presents comparisons of the weights of all fully optimized panels.

For both the pyramidal and the transverse corrugated sheet panel (Fig. 8(a) and (c)), the optimal angle initially diminishes gradually with load, then drops rather precipitously over a narrow load range (the rate change being associated with a change in the mechanism combination), and finally saturates at a fixed value, 45° , in the high load domain. (The latter result was the basis for the selection of this angle in the three-parameter optimization calculations, presented in Figs. (4), (5) and (7).) The same trends are obtained for all yield strains, with only a shift in the critical loads at the mechanism transitions. The tetrahedral truss core panel exhibits broadly the same trends, except for an additional mechanism domain for low yield strains in which the optimal angle increases (rather than decreases) with load. In the high load domain, the optimal angle also saturates at 45° (again, the basis for its selection in the three-parameter optimization). For the longitudinal corrugated panel, the variation in optimal angle with load begins in the same manner, but then reaches a fixed value, 50.8° , over a narrow load range, and subsequently rises rapidly with load. In this case, an angle of 45° is never optimal. Finally, for the honeycomb core, the optimal cell aspect ratio increases with load, from about 0.2 to 1. Thereafter, its value is non-unique. Instead, for reasons detailed in Appendix A, the optimal design is independent of ξ , provided it does not exceed a prescribed maximum, plotted as the dotted lines in Fig. 9(e). Based on these results, an intermediate value of 0.5 was selected for the preceding three-parameter optimizations.

Interestingly, the panels obtained through the three-parameter optimization are only slightly heavier than the fully optimized panels, provided ξ or θ are selected judiciously. For the pyramidal, tetrahedral and corrugated panels, the results for $\theta = 45^\circ$ appear to provide reasonable designs over the entire load range. In some instances, weight reduction can be obtained by changing the angle to a slightly higher value (70°), as illustrated in Fig. 9(d). For the honeycomb core panel, selecting ξ to be 0.5 yields design weights that are almost indistinguishable from the fully optimized panel.

The weight rankings of the fully optimized panels (Fig. 10) differ only slightly from those obtained through the three-parameter optimizations. Specifically, in the low load domain, the tetrahedral truss core panel is the lightest, followed closely by the honeycomb, pyramidal and longitudinal corrugated; the transverse corrugated remains the heaviest, by as much as a factor of 2. In the high load domain, the rankings essentially reverse, with the transverse corrugated being the lightest, although the weight differences remain small (<20%).

The panel weights are again found to be similar to one another in the high load domain. This is a consequence of two features of the optimal design: (i) the dominance of the face sheet weight, and (ii) the face sheet weight being independent of core topology (Appendix A). To demonstrate the former result, Fig. 11 shows the variation in the weight fraction associated with the core as a function of load. At high loads, the

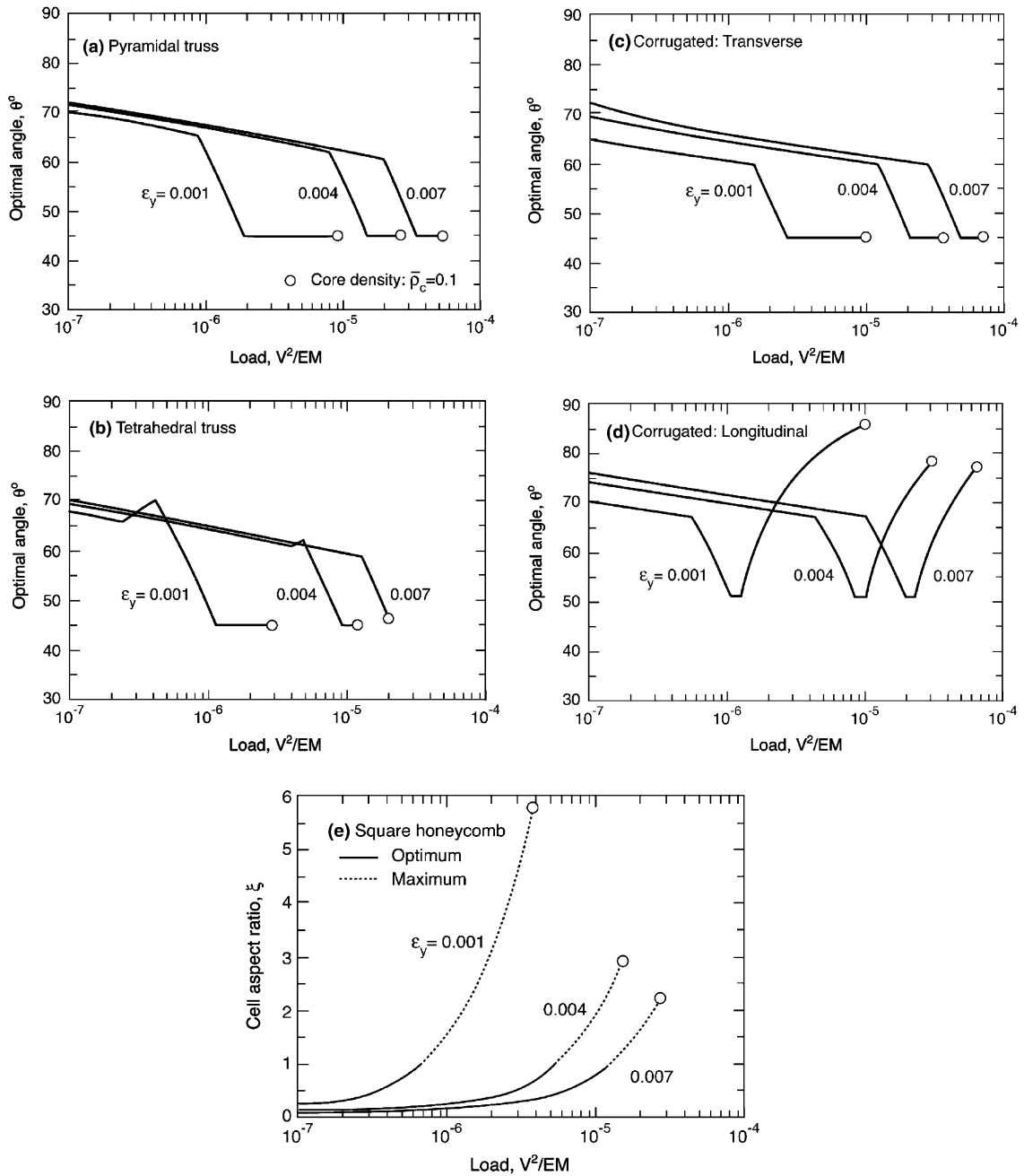


Fig. 8. Results of four-parameter optimizations, showing variation with load of (a–d) the optimal core member angles, θ , and (e) the core member aspect ratio, ξ , for the square honeycomb core ($\nu = 1/3$).

core constitutes between 17% and 34% of the total panel weight, depending on its topology: the balance (66–83%) coming from the face sheets. These differences reflect directly the shear yield strengths of the various cores. That is, the transverse corrugated core is the strongest, thereby yielding the lowest core weight

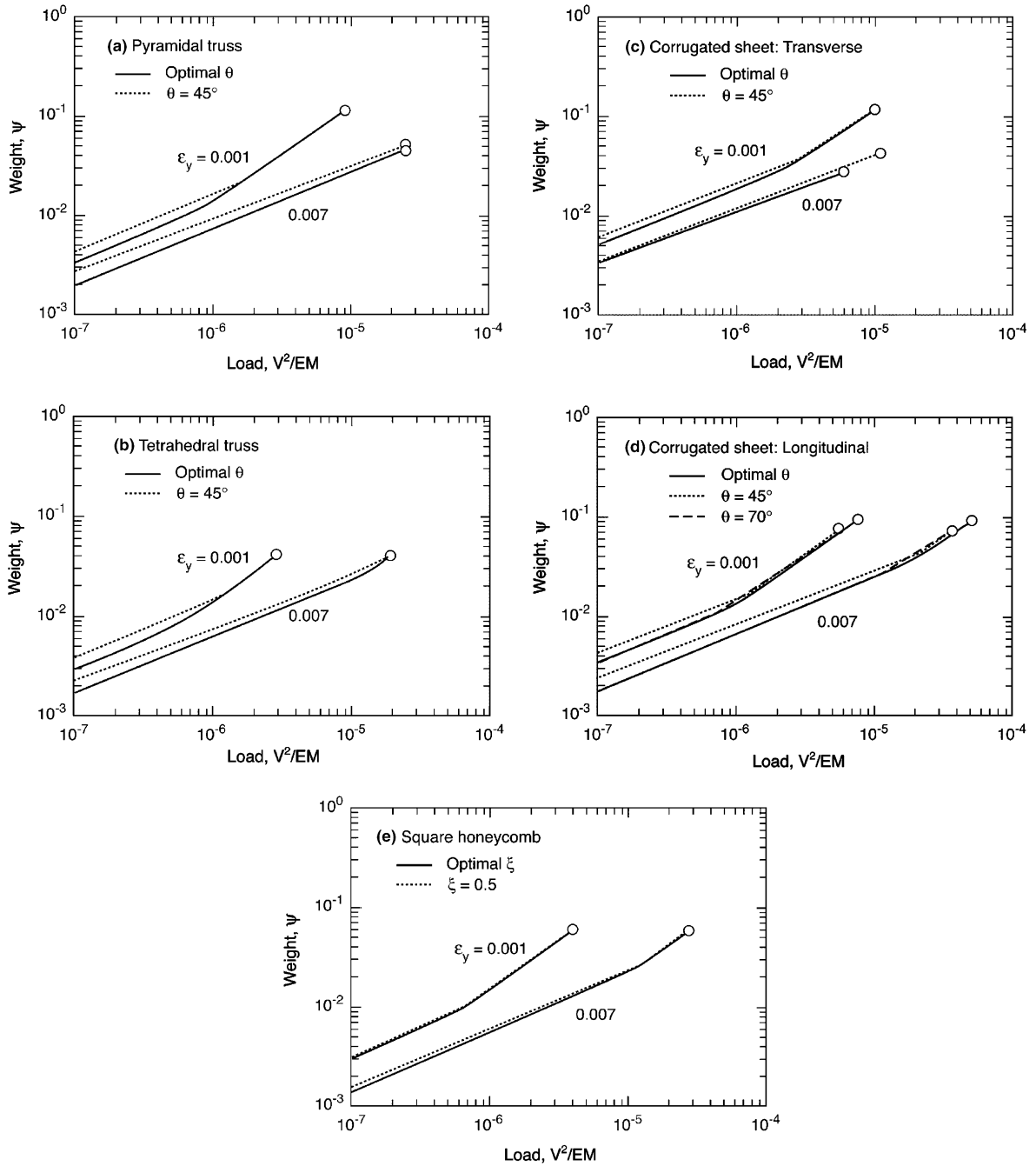


Fig. 9. Comparisons of three- and four-parameter optimizations ($\nu = 1/3$), for both low and high yield strain values.

fraction (17%) and the lowest panel weight (Fig. 10). In contrast, the square honeycomb core is the weakest (typically half that of the transverse corrugated) and hence exhibits both the highest core weight fraction (34%) and the highest panel weight (Fig. 10).

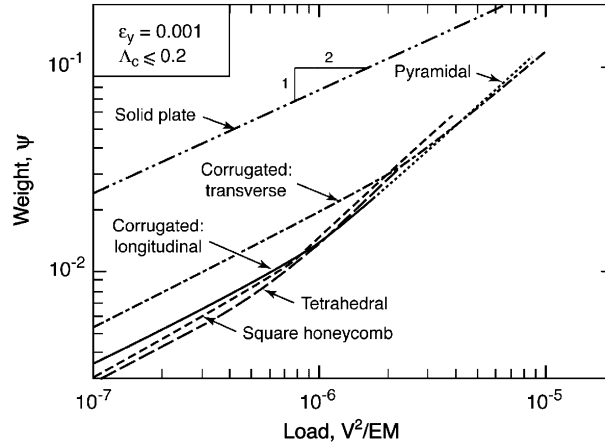


Fig. 10. Weight comparison of fully optimized sandwich panels ($\nu = 1/3$). The results for the pyramidal core panel (short dashed line) are virtually indistinguishable from those for the longitudinal corrugated core panel (solid line) in the low load domain.

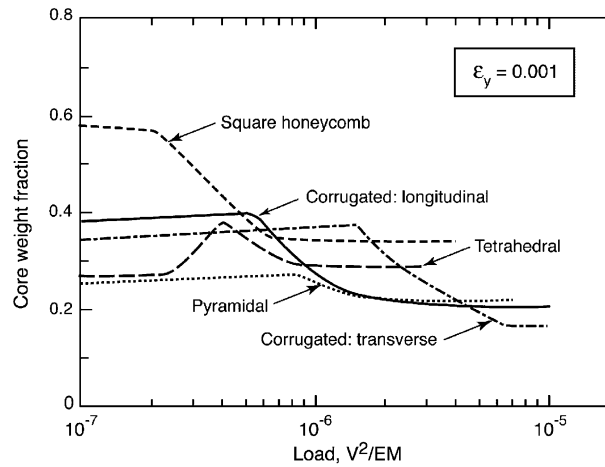


Fig. 11. Core weight fraction (relative to total panel weight) from four-parameter optimization.

The lack of dependence of face sheet weight on core topology at high loads can be understood through examination of the face yielding constraint (Eq. (8a)) coupled with the core thickness restriction ($\Lambda_c \leq \Lambda_c^0$). Since the face sheets support all of the bending moment and their separation distance is constant (dictated by the allowable core thickness, Λ_c^0), the load for yield initiation is proportional to face sheet thickness. Furthermore, since the face sheet weight is also proportional to face sheet thickness, it follows that the load is proportional to face sheet weight, independent of core topology. Indeed, as described in Appendix A, the optimal face sheet thickness at high loads is given by the same formula as that emerging from the three-parameter optimization (Eq. (23a)).

7. Concluding remarks

A methodology for the design of strong lightweight metallic sandwich panels has been described and implemented. For the four core topologies considered, the design constraints can be generalized in the form

of power law functions. When restricted to three independent parameters, the optimizations can be performed analytically, yielding closed-form solutions for the optimal values of the design parameters as well as the weight. The solutions provide insights into the trends in the design parameters with the load capacity and the material yield strain. In addition, they can be used readily for computations, for the purpose of assessing and comparing the various core topologies. The addition of a fourth independent parameter renders the problem too complex to yield closed-form solutions for all cases of interest. Instead, it leads to implicit functions for at least one of the design parameters. Consequently, numerical methods are required to obtain the optimal design. Alternatively, the four-parameter optimization can be performed by a direct numerical route, starting with the pertinent design constraints. In this case, the intermediate (implicit) analytical solutions are of marginal benefit.

The variations in the weights of the optimized panels are rather small, especially upon comparison with the weight of a solid panel. The similarities are particularly pronounced in the high load domain. At low loads, most panels perform similarly well, with weight variations of only about 15%. The one exception is the transverse corrugated core panel, which is almost twice as heavy as the others. On this basis, selection of core topology is expected to be dictated by considerations other than strength, such as manufacturing costs, as well as the potential for multifunctionality.

The present assessment for corrugated panels has the limitation that the longitudinal and transverse orientations have been considered separately. In many practical situations, they should be considered jointly. Then, the design is adjusted to find the lowest weight that supports load in both directions. This analysis, which will be reported in a subsequent article (Rathbun et al., in preparation), perhaps surprisingly, demonstrates that the jointly optimized panel is only slightly heavier than that ascertained from the results in this article.

Acknowledgement

This work was supported by the ONR MURI program on Blast Resistant Structures through a sub-contract from Harvard University to the University of California at Santa Barbara (Contract No. 123163-03).

Appendix A. Select solutions from four-parameter optimizations

Analytical solutions for ξ (or θ , via Eq. (7)) in the four-parameter optimizations have been obtained for each of the core topologies in Fig. 2. In many cases of interest, the solutions are in the form of implicit functions, precluding the development of explicit formulae for the other geometric parameters (λ_f , A_c , and λ_c) and the weight, Ψ . Numerical methods have been employed in parallel with the analytical approach, both to determine the active constraints in each loading domain and to verify the accuracy of the analytical solutions. To illustrate the procedure, the determination of the optimal truss angle, θ , for the pyramidal core is provided as an example. Finally, a unique feature of the optimal cell aspect ratio for the square honeycomb panel in the high load domain is discussed.

A.1. Four variable optimization of pyramidal truss core panel

For the pyramidal truss core panel in the *low load domain*, the active mechanisms are FY, FB, and CB. By setting the corresponding constraint functions (Eqs. (8a), (8b) and (8d)) equal to unity and incorporating the appropriate parameters from Table 3, Ψ can be written in terms of θ alone

$$\Psi = \left[\frac{384(1 - \nu^2)\Pi^2}{\pi^2 \varepsilon_y \tan^2 \theta} \right]^{1/4} + 3.9 \left[\frac{\Pi^6 \tan^{14} \theta}{\pi^6 (1 - \nu^2) \varepsilon_y^3 \sin^{20} \theta} \right]^{1/8} \quad (\text{A.1})$$

The value of θ that minimizes Ψ (determined by setting $\partial\Psi/\partial\theta = 0$) is given by the implicit formula

$$\left[\frac{24(1-v^2)\Pi^2}{\pi^2\varepsilon_y} \right]^{1/4} \frac{1}{(\tan\theta)^{3/2}\cos^2\theta} - 3.9 \left[\frac{\Pi^6}{\pi^6\varepsilon_y^3(1-v^2)} \right]^{1/8} \left\{ \frac{7(\tan\theta)^{3/4}}{4(\sin\theta)^{5/2}\cos^2\theta} - \frac{5(\tan\theta)^{7/4}\cos\theta}{2(\sin\theta)^{7/2}} \right\} = 0 \quad (\text{A.2})$$

Clearly, the optimal value of θ can be obtained only through a numerical route. The optimal values of A_c , λ_f and λ_c are then determined by setting the FY, FB and CB constraint functions equal to unity and combining the results with the computed value of θ .

For the fully optimized pyramidal core panel, there are *two intermediate load domains*. The first occurs once the core thickness reaches its maximum allowable value, $A_c = A_c^0$; the active mechanisms remain FY, FB and CB. With A_c^0 known, λ_f is determined by setting the FY constraint (Eq. (8a)) equal to unity. Combining this result with the FB constraint (Eq. (8b)) yields the optimal angle

$$\theta = \tan^{-1} \left\{ \left(\frac{24(1-v^2)\varepsilon_y^3}{\pi^2} \right)^{1/2} \frac{(A_c^0)^2}{\Pi} \right\} \quad (\text{A.3})$$

Then, λ_c is obtained by combining the preceding results with the CB constraint (Eq. (8d)). The second intermediate load domain arises through a mechanism transition, from CB to CY. Here, essentially the same procedure is used to obtain the optimal parameters. Interestingly, since the optimal angle is defined by a combination of the FY and FB constraints, and since both of these mechanisms are operative in these two domains, the solution for θ is the same: notably, that given by Eq. (A.3). The difference in the two arises in the optimal value of λ_c : in the latter domain, it is dictated by CY (Eq. (8c)), rather than CB.

In the *high load domain*, FB becomes inactive, leaving only FY and CY. Since the core thickness remains fixed at its maximum allowable value ($A_c = A_c^0$), λ_f and λ_c are determined by setting the FY and CY constraint functions equal to unity, respectively. With these parameters known, Ψ is written in terms of θ alone

$$\Psi = \frac{2\Pi}{\varepsilon_y A_c^0} + \frac{\sqrt{2}\Pi \tan\theta}{\varepsilon_y \sin^2\theta} \quad (\text{A.4})$$

By setting $\partial\Psi/\partial\theta = 0$, the optimal value of θ is found to be

$$\theta = \frac{\pi}{4} \quad (\text{A.5})$$

An analogous procedure was used for the other core topologies. The results are plotted in Fig. 8.

A.2. Square honeycomb panel in high load domain

For the square honeycomb panel in the high load domain, the active constraints are FY and CY, and $A_c = A_c^0$. Setting the constraint functions equal to unity allows elimination of λ_f and λ_c from the weight function, yielding the result

$$\Psi = \frac{2\Pi}{\varepsilon_y} \left[\frac{1}{A_c^0} + \frac{3\sqrt{3}}{2} \right] \quad (\text{A.6})$$

In this case, Ψ is *independent* of the cell aspect ratio, ξ . Consequently, there is no unique optimal value of ξ . Rather, the maximum value of ξ is dictated by the requirement that the FB constraint function (Eq. (8b)) does not exceed unity. This condition is satisfied when

$$\zeta \leq \left[\frac{3.3\Pi^2}{\varepsilon_y^3 (A_c^0)^4 (1 - \nu^2)} \right]^{1/2} \quad (\text{A.7})$$

The latter result is plotted as the dashed lines in Fig. 8(e).

References

- Ashby, M.F., Evans, A.G., Fleck, N.A., Gibson, L.J., Hutchinson, J.W., Wadley, H.N.G., 2000. *Metal Foams: A Design Guide*. Butterworth Heinemann, Boston.
- Chiras, S., Mumm, D.R., Evans, A.G., Wicks, N., Hutchinson, J.W., Dharmasena, K., Wadley, H.N.G., Fichter, S., 2002. The structural performance of near-optimized truss core panels. *International Journal of Solids and Structures* 39 (15), 4093–4115.
- Cote, F., Deshpande, V., Fleck, N.A., Evans, A.G., 2004. The out-of-plane compressive behavior of metallic honeycombs. *Materials Science and Engineering, A* 380 (1–2), 272–280.
- Deshpande, V.S., Fleck, N.A., 2001. Collapse of truss core sandwich beams in 3-point bending. *International Journal of Solids and Structures* 38 (36–37), 6275–6305.
- Deshpande, V.S., Fleck, N.A., Ashby, M.F., 2001. Effective properties of the octet-truss lattice material. *Journal of the Mechanics and Physics of Solids* 49, 1747–1769.
- Evans, A.G., Hutchinson, J.W., Fleck, N.A., Ashby, M.F., Wadley, H.N.G., 2001. The topological design of multifunctional cellular metals. *Progress in Materials Science* 46, 309–327.
- Fleck, N.A., Deshpande, V.S., 2004. The resistance of clamped sandwich beams to shock loading. *Journal of Applied Mechanics* 71 (3), 386–401.
- Hutchinson, R.G., Wicks, N., Evans, A.G., Fleck, N.A., Hutchinson, J.W., 2003. Kagorne plate structures for actuation. *International Journal of Solids and Structures* 40 (25), 6969–6980.
- Lu, T.J., Hutchinson, J.W., Evans, A.G., 2001. Optimal design of a flexural actuator. *Journal of Mechanics and Physics of Solids* 49 (9), 2071–2093.
- Qiu, X., Deshpande, V.S., Fleck, N.A., 2003. Finite element analysis of the dynamic response of clamped sandwich beams subject to shock loading. *European Journal of Mechanics A—Solids* 22 (6), 801–814.
- Rathbun, H.J., Wei, Z., He, M.Y., Zok, F.W., Evans, A.G., Sypeck, D.J., Wadley, H.N.G., 2004. Measurement and simulation of the performance of a lightweight metallic sandwich structure with a tetrahedral truss core. *Journal of Applied Mechanics* 71 (5), 368–374.
- Rathbun, H.J., Wei, Z., Zok, F.W., McMeeking, R.M., Evans, A.G., 2005. Analysis and strength optimization of sandwich beams with honeycomb cores, in preparation.
- Sypeck, D.J., Wadley, H.N.G., 2002. Cellular metal truss core sandwich structures. *Advanced Engineering Materials* 4 (10), 759–764.
- Wadley, H.N.G., Fleck, N.A., Evans, A.G., 2003. Fabrication and structural performance of periodic cellular metal sandwich structures. *Composites Science and Technology* 63 (16), 2331–2343.
- Wicks, N., Hutchinson, J.W., 2001. Optimal truss plates. *International Journal of Solids Structures* 38, 6165–6183.
- Wicks, N., Hutchinson, J.W., 2004. Performance of sandwich plates with truss cores. *Mechanics of Materials* 36 (8), 739–751.
- Xue, Z.Y., Hutchinson, J.W., 2003. Preliminary assessment of sandwich plates subject to blast loads. *International Journal of Mechanical Sciences* 45 (4), 687–705.
- Zok, F.W., Rathbun, H.J., Wei, Z., Evans, A.G., 2003. Design of metallic textile core sandwich panels. *International Journal of Solids Structures* 40, 5707–5722.
- Zok, F.W., Waltner, S.A., Wei, Z., Rathbun, H.J., McMeeking, R.M., Evans, A.G., 2004. A protocol for characterizing the structural performance of metallic sandwich panels: application to pyramidal truss cores. *International Journal of Solids and Structures* 41, 6249–6271.
- Zok, F.W., Rathbun, H.J., He, M.Y., Ferri, E., Mercer, C., McMeeking, R.M., Evans, A.G., in press. Structural performance of metallic sandwich panels with square honeycomb cores. *Philosophical Magazine*.